Chinese Chemical Letters 35 (2024) 108459

Contents lists available at ScienceDirect

Chinese Chemical Letters

journal homepage: www.elsevier.com/locate/cclet

Pt/Mo chalcogenide composite deriving from Pt-Mo_6S_8 by high temperature shock for enhanced HER performance

Meng Liu[a], Guocheng Lv[a,*], Hao Liu[b], Tianming Liu[b], Lingchang Kong[a], Libing Liao[a,*]

[a] Engineering Research Center of Ministry of Education for Geological Carbon Storage and Low Carbon Utilization of Resources, Beijing Key Laboratory of Materials Utilization of Nonmetallic Minerals and Solid Wastes, National Laboratory of Mineral Materials, School of Materials Science and Technology, China University of Geosciences (Beijing), Beijing 100083, China
[b] School of Science, China University of Geosciences, Beijing 100083, China

ARTICLE INFO

Article history:
Received 7 March 2023
Revised 2 April 2023
Accepted 14 April 2023
Available online 16 April 2023

Keywords:
HTS
Low Pt loading
Mo_6S_8
$MoS_2/MoO_2/Mo_6S_8$ composite
HER

ABSTRACT

Highly efficient catalysts for electrolysis of water are crucial to the development of hydrogen energy which is helpful to carbon neutralization. Recently, high temperature shock (HTS), with advantage of rapid speed, universality and scalable production, has been a promising method in synthesis of nanomaterials. In this paper, HST was used to treat low Pt loading Mo_6S_8 for enhanced water splitting performance. Impressively, the optimized $MoS_2/MoO_2/Mo_6S_8$ nano-composite with low Pt mass loading (~4%) displays well hydrogen evolution reaction (HER) electrochemical performance. The overpotential is 124 mV to reach 10 mA/cm^2 and the corresponding Tafel slope is 88 mV/dec in acidic electrolyte. Its mass activity is 6.2 mA/μg_{Pt} at -124 mV *vs.* RHE, which is almost 2 times relative to 20% Pt/C. Moreover, it presents distinguished stability even after 2000 cycles. This work will broaden the way of catalysts preparation and the application of hydrogen evolution.

It is more urgent to deal with the climate change problems and reduce carbon dioxide emissions [1]. Carbon peak and carbon neutrality have received more attention in recent years. Hydrogen has become one of the most promising alternative clean sources which is comparable with fossil fuels without any carbon dioxide emission [2,3]. Electrolysis of water has become one of the most efficient ways in hydrogen and oxygen energy production [4,5]. In the process of electrolysis of water, catalysts with highly electrochemical activity and stability are crucial for water splitting [6,7]. For now, Pt is deemed to be the most efficient catalyst for HER. However, the scarcity and high costs have hindered the application of Pt [8,9]. Therefore, exploitation of catalysts without Pt or using little Pt has become research hotspot [10–12].

Chevrel phase compounds are a group of inorganic materials that can play important roles in electrochemical energy storge and electro-catalysis due to the unique crystal structure and properties. Different kinds of electrochemical reduction reactions can be found on Cheverl phases (CPs, $Mo_{6\times8}$) [13,14]. The structure of CPs is highly tunable [15], in which the electronic structures are versatile with different charge transfer performance (Fig. S1a in Supporting information). Moreover, the biggest characteristic of CPs is its high electronic conductivity, which is because the delocalized metallic bonds in the Mo_6 cluster, resulting in the metal-like properties [16]. The metal-like properties of CPs are favorable for the electrochemical reduction reactions, which is similar to 1T MoS_2 [17,18]. Meanwhile, low-coordinated Mo-S in MoS_2 (Fig. S1b in Supporting information) exhibits low hydrogen adsorption free energy [19], of which the HER performance can be close to Pt in acidic media in theory [20]. Nevertheless, the rate-determining step is affected by the energy barrier during the process [21]. A large number of researches show that the energy barrier of water dissociation on MoO_2 (Fig. S1c in Supporting information) is relatively low [22–24]. Considering the low hydrogen adsorption free energy of MoS_2, low water dissociation of MoO_2 and high electroconductibility of Mo_6S_8, the combination of the abovementioned materials seems to be a feasible mean for improving HER performance. In addition, the highly efficient catalytic performance of Pt is undeniable [25]. Therefore, preparation of catalysts with low Pt loading or Pt-free is a desired orientation in developing HER performance [26]. Commonly, the preparation of nano-size Pt or large surface area and high stability carrier with low Pt is the main means to reduce the application amount of Pt [27,28]. Various substrates such as carbon [29], MXenes [30], sulfide [31], and heterojunction [32]. Besides, different kinds of metal sulfide [33–35], oxide [36–38], cobalt-based compound [39] and metal-free catalysts

* Corresponding authors.
E-mail addresses: guochenglv@cugb.edu.cn (G. Lv), clayl@cugb.edu.cn (L. Liao).

https://doi.org/10.1016/j.cclet.2023.108459
1001-8417/

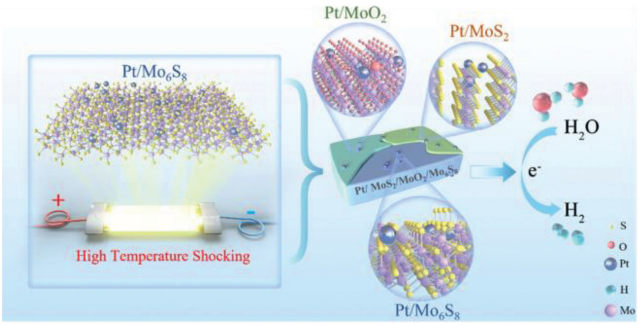

Fig. 1. Schematic illustration of preparation and action mechanism of $Pt/MoS_2/MoO_2/Mo_6S_8$.

[40] have been developed over wide pH values. Meanwhile different technologies for overall water splitting have also been carried out [41–43]. Studies in recent years have shown that the MoO_2 and MoS_2 based composites are mainly prepared by hydrothermal or high temperature solid sintering methods, which require high temperature and long duration [23,44,45]. However, the traditional methods are hash and dangerous which is not fitting the conditions of industrial manufacturing [46]. Chen *et al*. first reported an ultra-fast and simple synthesis method for nanomaterials by Joule heating [47–50], which provide a new horizon in nanomanufacturing [51–54]. Herein, we demonstrated our findings on low loading of Pt as decoration to Mo_6S_8. The following ultra-fast HTS method (Fig. S2 in Supporting information) was introduced to obtain nanocomposites of $Pt/MoS_2/MoO_2/Mo_6S_8$ for the first time with enhanced HER performance, which provide a fast synthetic method in nano-composites. Schematic illustration of preparation and action mechanism was presented in Fig. 1. $Pt/MoS_2/MoO_2/Mo_6S_8$ nanocomposite was derived from Pt/Mo_6S_8 by one-step HTS, which was used in the following tests.

As shown in Fig. S3a (Supporting information), the crystalline phase of Mo_6S_8 was characterized by XRD. The peaks of XRD pattern matches well with space group of $R\bar{3}$ space group (PDF#24–0319) with $a = b = 9.1833(3)$ Å and $c = 10.8716(5)$ Å [55]. And it displayed a size of several hundred nanometers (200–1000 nm) in length width (Fig. S3b in Supporting information). After Pt loading (the loading amount described in the figure is feed ratio rather than practical loading, which will be identified by ICP), the diffraction peaks also can be well matched to PDF#24–0319, while with broadening of peaks as shown in Fig. S4a (Supporting information), which indicating the declining in particles sizes. It also can be found in Fig. S5 (Supporting information) that after loading Pt, the size of Mo_6S_8 becoming smaller and Pt particles can be detected in SEM with uniform element distribution and trace Pt can be detected in mapping. 10% Pt/Mo_6S_8 was selected to be treated by HTS. As shown in Fig. S4b (Supporting information, the MoO_2 (PDF#32–0671), MoS_2 (PDF#37–1492) and Mo_6S_8 (PDF#27–0319) can be observed, indicating the synthesis of $MoS_2/MoO_2/Mo_6S_8$ composite in the system.

The SEM and HRTEM images of $Pt/MoS_2/MoO_2/Mo_6S_8$ catalyst were showed in Figs. 2a and b. The feed ratio of 10% Pt nanoparticles decorated on $MoS_2/MoO_2/Mo_6S_8$ ($Pt/MoS_2/MoO_2/Mo_6S_8$) can be seen and a number of ultra-fine Pt nanoparticles can be seen which has been distributed uniformly on the base. After HTS, the particles are mostly reduced into 100 nm, the size of which is smaller compared to the ones in Fig. S5a. The HRTEM image in Fig. 2c proves the heterostructure of MoS_2 and MoO_2 with two clear diffraction lattice stripes 0.202 nm and 0.240 nm, attributing to (006) lattice plane of MoS_2 and (200) lattice plane of MoO_2. And Pt particles can be clearly seen anchoring on the base. The lamellar structure can be observed in Fig. 2d and the diffraction lattice stripes is about 0.64 nm, corresponding to Mo_6S_8 with a characteristic plane of (101). The selected regions in the HRTEM image were further analyzed by Fast Fourier Transform and Inverse Fast Fourier Transform (inset), which reveals clear diffraction lattice stripes with 0.23 nm, which is corresponding to (111) diffraction lattice stripe of Pt. Meanwhile, the defect of Mo_6S_8 and ultra-thin lamella loading nano Pt particles can be observed in the edge of the bulk materials (Figs. 2e–h). The EDX elemental mapping images in Fig. 2i indicated the homodisperse of Mo, S, O and Pt elements in $Pt/MoS_2/MoO_2/Mo_6S_8$ catalyst. Especially, Pt particles distribution on the base is clear. The results in Fig. S6 (Supporting information) showed that the mass fraction of Pt is about 6.73%, which is close to the result of ICP-OES result of ~4%.

These valence states of $Pt/MoS_2/MoO_2/Mo_6S_8$ were estimated by XPS. The elements of Mo, S, O and Pt can be detected on the surface of catalyst in Fig. S7a (Supporting information). While in Fig. S8a (Supporting information), the element of O is not found, which is consistent to the results of XRD. Figs. S7b and c (Supporting information) were the XPS spectra of Mo 3d and S 2p. The peaks of Mo 3d which were at 228.0 eV and 231.1 eV indicated the delocalized metallic bonds (Mo-Mo). And Mo^{4+} and Mo^{6+} also have been also detected, in which Mo^{4+} is corresponding to the Mo in MoO_2 and MoS_2, while Mo^{6+} may be due to the surface oxidation. The characteristic peak of Mo-S for MoS_2 can be detected clearly at 226.1 eV in Fig. S7b, which is different from the Mo state of the unshocked in Fig. S8b (Supporting information). The S 2p XPS shows that there are two peaks at 163.1 eV and 161.8 eV go with S $2p_{1/2}$ and S $2p_{3/2}$ corresponding to S^{2-} (Fig. S7c). And before shocking, the S remains parts of the valence between −2 and 0, which mostly belongs to Mo_6S_8 phase (Fig. S8c in Supporting information). The Pt 4f XPS was shown in Fig. S7d (Supporting information). It can be seen that Pt 4f splits into two peaks at 71.25 eV (Pt $4f_{7/2}$) and 74.80 eV (Pt $4f_{5/2}$), corresponding to metallic Pt^0. Moreover, before shocking, another pair of peaks were detected at 72.09 eV and 75.12 eV, which belongs to Pt^{2+} (Fig. S8d in Supporting information), indicting after shocking, parts of Pt^{2+} has been reduced to Pt^0 [25].

The liner sweep voltammetry (LSV) curves was tested to evaluate the overpotential of different Pt loading amount Mo_6S_8 in Fig. 3a. The overpotential at 10 mA/cm^2 was used to compare the activity of the catalysts. The catalysts treated with different process show different HER activity. When the feed ratio is 10% (practical amount of 4%), the Pt/Mo_6S_8 catalyst exhibits smaller overpotential of 190 mV than the Mo_6S_8 catalyst of 320 mV. Then different time of HTS treating was applied to treat the catalyst of 10% Pt/Mo_6S_8. As shown in Fig. S9 (Supporting information), when the treating time of HTS is 30 s, the HER performance has been improved a lot compared with the other treating time of the catalysts. As shown in Fig. S10 (Supporting information), lager granular sizes of the base and loading Pt particles are induced by long HTS treating time, indicating decreased active specific surface area, leading to severe activity loss. After 800 °C high temperature shocking for 30 s (labeled as $Pt/MoS_2/MoO_2/Mo_6S_8$), the overpotential has been further reduced to 124 mV (Fig. 3b). Moreover, its mass activity is 6.2 mA/μg$_{Pt}$ at −124 mV *vs*. RHE, almost 2 times relative to 20% Pt/C. The HER performance of different Pt/substrates was investigated in Fig. S11 (Supporting information). It can be seen that among three kinds of Pt/substrates with the same initial feed quantity (10%), Pt/MoO_2 exhibits lower overpotential than Pt/MoS_2 and Pt/Mo_6S_8. While $Pt/MoS_2/MoO_2/Mo_6S_8$ still exhibits the lowest overpotential, which may due to the defects and MoO_2/MoS_2 heterostructure in the composite. Besides, as shown in Fig. S12 (Supporting information), $Pt/MoS_2/MoO_2/Mo_6S_8$ exhibits lower overpotential of 150 mV compared with the catalysts of Mo_6S_8 and Pt/Mo_6S_8 under basic electrolyte. And the stability under basic electrolyte is inferior to acid electrolyte.

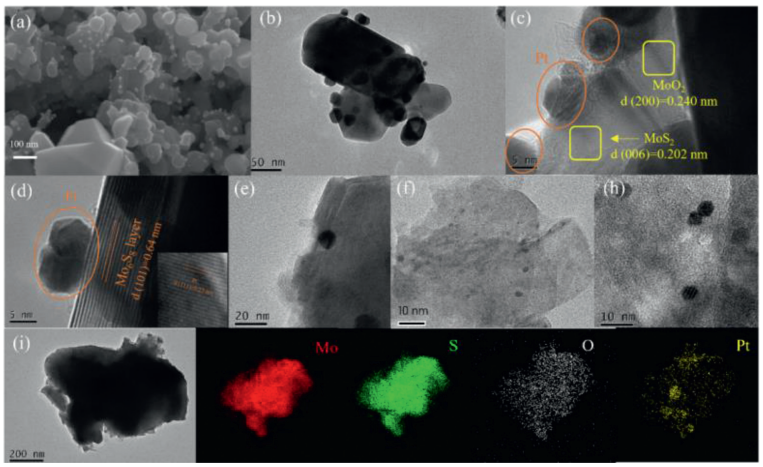

Fig. 2. (a) SEM image of $Pt/MoS_2/MoO_2/Mo_6S_8$. (b–h) HRTEM images of $Pt/MoS_2/MoO_2/Mo_6S_8$. (i) EDS-mapping of $Pt/MoS_2/MoO_2/Mo_6S_8$.

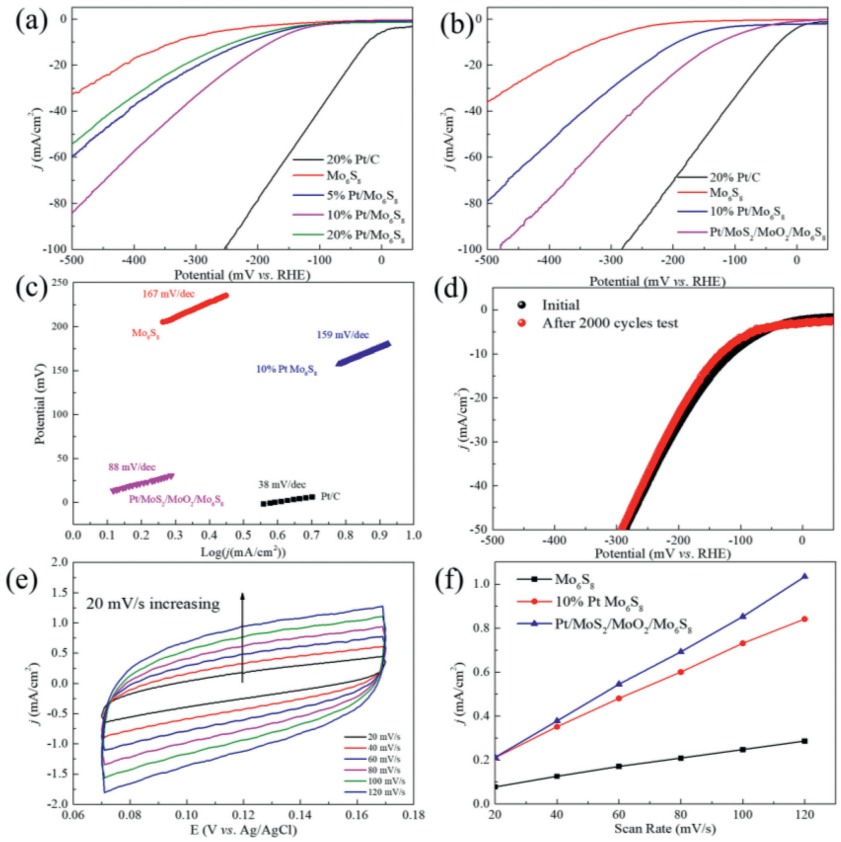

Fig. 3. (a) LSV curves of different Pt loadings of Mo_6S_8 catalysts. (b) Comparison of LSV curves of different catalysts. (c) Comparison of Tafel slope of different catalysts. (d) LSV curve after 2000 cycles. (e) CV curves of $Pt/MoS_2/MoO_2/Mo_6S_8$ at different potential scanning rates. (f) Linear fitting of the currents of Pt/ $MoS_2/MoO_2/Mo_6S_8$ *vs.* scan rates.

HER kinetics was evaluated by Tafel slope, which can be got by fitting the Tafel equation ($\eta = a + b\log j$) [56]. The Tafel slope of $Pt/MoS_2/MoO_2/Mo_6S_8$ (88 mV/dec) is smaller than Mo_6S_8 (167 mV/dec) and Pt/Mo_6S_8 (159 mV/dec) in Fig. 3c. The smaller Tafel slope of $Pt/MoS_2/MoO_2/Mo_6S_8$ compared with Mo_6S_8 and Pt/Mo_6S_8 illustrates that the HER velocity of $Pt/MoS_2/MoO_2/Mo_6S_8$ was faster when the overpotential increases. There are three kinds of reactions involved in hydrogen evolution mechanism. The mechanisms that affect the HER process are mainly Tafel reaction, Heyrovsky reaction and Volmer reaction, when the Tafel slope is 30, 40, 120 mV/dec. The catalyst of $Pt/MoS_2/MoO_2/Mo_6S_8$ with Tafel slope of 88 mV/dec indicates that the HER was determined by the Volmer-Heyrovsky mechanism, suggesting that the Volmer reaction is the rate-determining step and in this reaction protons were converted to the adsorbed hydrogen atoms [57].

Another important indicator to evaluate the electrochemical catalysts is the stability. The HER performance after 2000 CV cycles was shown in Fig. 3d. There is no attenuation in LSV curve of the catalyst compared with the one before cycles, suggesting anchoring of Pt is strong on the surface of $MoS_2/MoO_2/Mo_6S_8$ base.

The effective surface area (ECSA) test was also used to evaluate the activity of catalysts, which can be obtained by testing CV curves under different scan rates. The corresponding CV curves were measured under different scan rates ranging from 20 mV/s

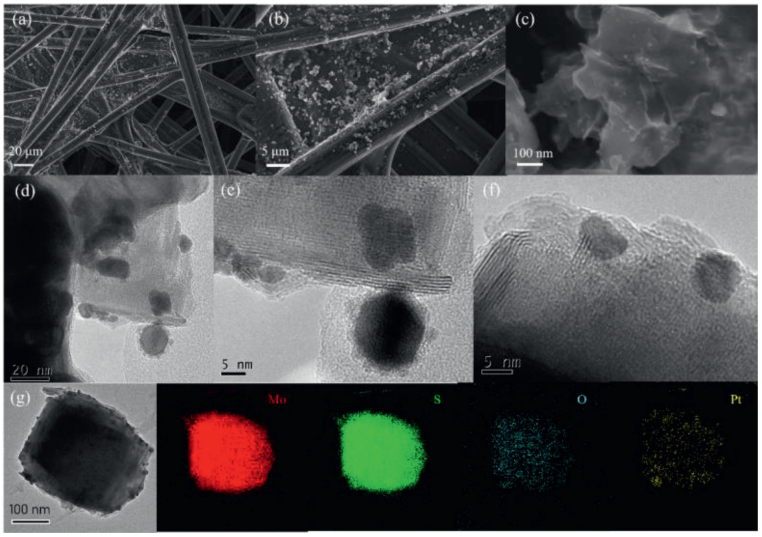

Fig. 4. (a–c) SEM images, (d–f) HRTEM images, (g) EDS-mapping of Pt/ $MoS_2/MoO_2/Mo_6S_8$ after 2000 CV cycles.

to 120 mV/s in potential range of 0.07–0.17 V *vs.* SCE where no Faraday reaction is reacted (Figs. 3d and e, Fig. S13 in Supporting information). C_{dl} can be calculated through the *j* obtained at 0.12 V *vs.* SCE in CV and scan rates curves from Fig. 3f. The slope of the curve *j* is twice of C_{dl} [58]. The C_{dl} of $Pt/MoS_2/MoO_2/Mo_6S_8$ is 7.8 mF/cm^2, demonstrating the maximum amounts of active sites, more than those of Pt/Mo_6S_8 (6.15 mF/cm^2) and Mo_6S_8 (2.01 mF/cm^2). Thus, it deems that the higher ECSA can be partly attributed to the nanostructure, and the other reason is that the heterostructure and defects in $Pt/MoS_2/MoS_2/Mo_6S_8$ can facilitate the electron transfer.

To further elucidate the properties of the catalysts, the morphology and element distribution of $Pt/MoS_2/MoO_2/Mo_6S_8$ after 2000 cycles operation were analyzed. The SEM images shows that Pt/ $MoS_2/MoO_2/Mo_6S_8$ catalyst has been distributed on the carbon paper uniformly (Figs. 4a and b). The layered morphology of Pt/ $MoS_2/MoO_2/Mo_6S_8$ is still preserved, and the Pt nano particles can be observed clearly (Fig. 4c). At the same time, the anchoring of Pt nano-particles can be also detected in the HRTEM images (Figs. 4d–f). The results of EDS-mapping indicated that the elements distribution is homogeneous and clearly Pt particles can be detected by mapping (Fig. 4g). The mass amount of Pt detected in EDS is 10.56% (Fig. S14 in Supporting information) without decreasing, indicating the high stability of the catalyst. Moreover, as shown in Fig. S15 (Supporting information), even after 100 h electrolysis the intact morphology of $Pt/MoS_2/MoO_2/Mo_6S_8$ is still preserved, and the Pt nano particles can be observed clearly. And XPS of the catalyst after cycling was carried out to confirm the valence change during HER. As shown in Fig. S16 (Supporting information), it can be seen that the valence states of S and Pt are remain the same. While Mo^{6+} which may be due to the surface oxidation has been disappeared during HER process, indicating the high stability of the catalyst.

In summary, a novel $MoS_2/MoO_2/Mo_6S_8$ nano-composite with low Pt loading (4%) was synthesized by ultra-fast HST for HER performance. The obtained $Pt/MoS_2/MoO_2/Mo_6S_8$ nano-composite displays well HER electrochemical performance with overpotential of 124 mV and a Tafel slope of 88 mV/dec. Volmer reaction is the main influence factor in the HER process. Strikingly, the mass activity is 6.2 $mA/\mu g_{Pt}$ at −124 mV *vs.* RHE, almost 2 times relative to 20% Pt/C. Moreover, $Pt/MoS_2/MoO_2/Mo_6S_8$ exhibits high stability with no decay in LSV after 2000 cycles and the integrity was observed in morphology after cycles. The work in this study may provide new avenues to develop highly efficient noble metal-doped nano composites in electrochemistry.

Declaration of competing interest

The authors declare there is no competing financial interests or personal relationships in this paper.

Acknowldgments

This work was supported by Beijing Natural Science Foundation (No. 2232062) and National Natural Science Foundation of China (No. 21875223).

Supplementary materials

Supplementary material associated with this article can be found, in the online version, at doi:10.1016/j.cclet.2023.108459.

References

[1] Y. Wang, M. Zhang, Y. Liu, et al., Adv. Sci. 10 (2023) 2207519.
[2] D. Hou, W. Zhou, X. Liu, et al., Electrochim. Acta 166 (2015) 26–31.
[3] Y. Pang, S. Zhu, Z. Cui, et al., Prog. Nat. Sci. Mater. 31 (2021) 201–206.
[4] J. Li, M. Guo, X. Yang, et al., Prog. Nat. Sci. Mater. 32 (2022) 705–714.
[5] X. Jin, Y. Xie, C. Zhao, et al., Prog. Nat. Sci. Mater. 31 (2021) 527–535.
[6] H. Wei, J. Si, L. Zeng, et al., Chin. Chem. Lett. 34 (2023) 107144.
[7] H.J. Qiu, Y. Ito, W. Cong, et al., Angew. Chem. Int. Ed. 54 (2015) 14031–14035.
[8] Y. Luo, D. Huang, M. Li, et al., Electrochim. Acta 219 (2016) 187–193.
[9] W.J. Liu, H. Jiang, H.Q. Yu, Energy Environ. Sci. 12 (2019) 1751–1779.
[10] X. Jian, M. Zhang, R. Li, et al., Electrochim. Acta 411 (2022) 140091.
[11] M. Yang, J. Zhang, W. Zhang, Z. Wu, F. Gao, J. Alloy. Compd. 823 (2020) 153790.
[12] X. Xie, Y.F. Jiang, C.Z. Yuan, et al., J. Phys. Chem. C 121 (2017) 24979–24986.
[13] J.C. Ortiz-Rodríguez, J.M. Velázquez, Curr. Opin. Electrochem. 34 (2022) 101002.
[14] P. Yu, Y. Xia, X. Feng, et al., Prog. Nat. Sci. Mater. 32 (2022) 739–744.
[15] M. Liu, G. Lv, T. Liu, et al., Prog. Nat. Sci. Mater. 33 (2023) 8–15.
[16] Y. Tong, A. Gao, Q. Zhang, et al., Energy Storage Mater. 37 (2021) 87–93.
[17] K. Qi, X. Cui, L. Gu, et al., Nat. Commun. 10 (2019) 5231.
[18] J. Cao, J. Zhou, M. Li, et al., Chin. Chem. Lett. 33 (2022) 3745–3751.
[19] L. Zhang, J. Liang, Y. Wang, et al., Angew. Chem. Int. Ed. 133 (2021) 25467–25472.
[20] X. Zhang, Z. Du, X. Luo, et al., Appl. Surf. Sci. 433 (2018) 723–729.
[21] R.D. Nikam, A.Y. Lu, P.A. Sonawane, et al., ACS Appl. Mater. Interfaces 7 (2015) 23328–23335.
[22] F. Gong, M. Liu, S. Ye, et al., Adv. Funct. Mater. 31 (2021) 2101715.
[23] L. Yang, W. Zhou, D. Hou, et al., Nanoscale 7 (2015) 5203–5208.
[24] J. Strachan, A.F. Masters, T. Maschmeyer, Mater. Res. Bull. 139 (2021) 111286.
[25] J. Zhao, Y. Zeng, J. Wang, et al., Nanoscale 12 (2020) 15393–15401.
[26] I.J. Hsu, Y.C. Kimmel, X. Jiang, B.G. Willis, J.G. Chen, Chem. Commun. 48 (2012) 1063–1065.

[27] T. Liu, W. Gao, Q. Wang, et al., Angew. Chem. Int. Ed. 132 (2020) 20603–20607.
[28] S. Hong, J.H. Kim, D. Shin, et al., Appl. Surf. Sci. 610 (2023) 155523.
[29] M. Tavakkoli, N. Holmberg, R. Kronberg, et al., ACS Catal. 7 (2017) 3121–3130.
[30] Y. Wu, W. Wei, R. Yu, et al., Adv. Funct. Mater. 32 (2022) 2110910.
[31] W. Ren, H. Zhang, C. Cheng, Electrochim. Acta 241 (2017) 316–322.
[32] B. Dong, Y.N. Zhou, J.C. Zhou, et al., Fuel 324 (2022) 124343.
[33] J. Chen, L. Zhang, J. Li, et al., J. Mater. Chem. A 11 (2023) 1116–1122.
[34] M. Zhang, Y. He, D. Yan, et al., Nanoscale 11 (2019) 22255–22260.
[35] A. Wang, M. Zhang, H. Li, et al., J. Phys. Chem. C 123 (2019) 13428–13433.
[36] H. Han, Y. Qiu, H. Zhang, et al., Sustain. Energy Fuels 6 (2022) 3008–3013.
[37] L. Ouyang, X. He, Y. Sun, et al., Inorg. Chem. Front. 9 (2022) 6602–6607.
[38] Y. Qiu, Z. Liu, Q. Yang, et al., Chem. Eur. J. 28 (2022) e202200683.
[39] X. Fang, X. Wang, L. Ouyang, et al., Molecules 27 (2022) 7617.
[40] Q. Liu, S. Sun, L. Zhang, et al., Nano Res. 15 (2022) 8922–8927.
[41] K. Zhang, X. Liang, L. Wang, et al., Nano Res. Energy 1 (2022) e9120032.
[42] L. Han, J. Xu, Y. Huang, W. Dong, X. Jia, Chin. Chem. Lett. 32 (2021) 2263–2268.
[43] X.P. Li, C. Huang, W.K. Han, T. Ouyang, Z.Q. Liu, Chin. Chem. Lett. 32 (2021) 2597–2616.
[44] Y. Li, C. Wang, M. Cui, et al., Appl. Surf. Sci. 543 (2021) 148804.
[45] C.L. Wu, P.C. Huang, S. Brahma, J.L. Huang, S.C. Wang, Ceram. Int. 43 (2017) S621–S627.
[46] H. Wu, Q. Lu, J. Zhang, et al., Nano-Micro Lett. 12 (2020) 1–12.
[47] S. Liu, Z. Hu, Y. Wu, et al., Adv. Mater. 32 (2020) 2006034.
[48] S. Dou, J. Xu, X. Cui, et al., Adv. Energy Mater. 10 (2020) 2001331.
[49] R. Jiang, Y. Da, X. Han, et al., Cell Rep. Phys. Sci. 2 (2021) 100302.
[50] C. Zeng, C. Duan, Z. Guo, et al., Prog. Nat. Sci. Mater. 32 (2022) 786–792.
[51] Y. Chen, G.C. Egan, J. Wan, et al., Nat. Commun. 7 (2016) 12332.
[52] S. Liu, Y. Shen, Y. Zhang, et al., Adv. Mater. 34 (2022) 2106973.
[53] C. Liu, Y. Shen, J. Zhang, et al., Adv. Energy Mater. 12 (2022) 2103505.
[54] C. Liu, W. Zhou, J. Zhang, et al., Adv. Energy Mater. 10 (2020) 2001397.
[55] J. Tarascon, F. Disalvo, D. Murphy, et al., J. Solid State Chem. 54 (1984) 204–212.
[56] S. Li, L. Zhao, S. Lei, et al., Nanoscale 12 (2020) 5003–5013.
[57] J. Tian, C. Yang, Z. Liu, et al., New J. Chem. 45 (2021) 19826–19830.
[58] J. Li, B. Zhang, Q. Song, X. Xu, W. Hou, Ceram. Int. 46 (2020) 14178–14187.